Multiphonon resonant Raman scattering in ZnO crystals and nanostructured layers

V. V. Ursaki, I. M. Tiginyanu,* V. V. Zalamai, and E. V. Rusu
Laboratory of Low-Dimensional Semiconductor Structures, Institute of Applied Physics of the Academy of Sciences of Moldova, Technical University of Moldova, MD-2004 Chisinau, Moldova

G. A. Emelchenko, V. M. Masalov, and E. N. Samarov
Laboratory of Crystallization from High-Temperature Solutions, Institute of Solid State Physics, 142432, Chernogolovka, Moscow district, Russia
(Received 23 April 2004; published 22 October 2004)

Multiphonon resonant Raman scattering (RRS) was studied in unintentionally doped bulk ZnO crystals and layers, including nanostructured and highly conductive films, excited by 351.1 and 363.8 nm laser lines in the temperature interval from 10 to 300 K. The variation of resonant conditions with sample temperature and wavelength of the excitation laser line allowed us to discriminate between the incoming and outgoing exciton mediated RRS by LO phonons. The quenching of luminescence and enhancement of Raman scattering in nanostructured ZnO layers grown on single-layer opals enabled us to observe the Raman signal in resonant configuration thus making possible to study multiphonon RRS by Fröhlich-type vibrational modes related to nanocrystallites with sizes less than 50 nm. The emission spectra of highly conductive ZnO films grown on porous InP substrates were found to consist of multiphonon RRS lines superimposed on a broad asymmetric near band gap photoluminescence (PL) band. The occurrence of PL and RRS in highly conductive layers is attributed to tailing of the density of states caused by potential fluctuations and to the breakdown of the wave-vector conservation due to randomly distributed impurities (intrinsic defects).

DOI: 10.1103/PhysRevB.70.155204 PACS number(s): 78.30.Fs, 78.55.Et, 78.66.Hf

I. INTRODUCTION

Zinc oxide (ZnO) is a promising material for manufacturing photodetectors, laser diodes for blue and ultraviolet spectral regions, transparent field effect transistors, etc.[1–3] In addition it proves to be suitable for the purpose of manufacturing room-temperature polariton lasers.[4] Transparent conductive oxide (TCO) thin-films consisting of ZnO offer a number of important advantages in comparison with conventionally used In, Sn, and Cd oxide coatings. In particular, they consist of cheap elements in contrast with In containing films; they are non-toxic in comparison with Cd containing films; the fundamental band gap of ZnO lies just at the high frequency border of the luminous spectrum therefore allowing tailoring of the ultraviolet absorption. Over the last years, a variety of ZnO nanostructures were fabricated such as nanocrystals, nanowires, nanocolumns, nanorods, nanotubes, nanocoral reefs, and ZnO-based hetero-opals exhibiting physical properties and good prospects for use in micro- and optoelectronics.

Resonant Raman scattering proves to be an important tool to get into the basic physical properties of semiconductors, including II-VI compounds. Note that RRS from solids can be observed if the energy of the incoming or scattered photons matches real electronic states in the material. One refers to incoming and outgoing resonance, respectively (see, e.g., Ref. 5). Multiphonon scattering processes were previously reported for single crystalline bulk ZnO,[6] and recently for ZnO films[7] and ZnO nanowires.[8] In all these cases the samples were excited by the 325 nm line of a He-Cd laser. The energy of this line is about 440 meV higher than the band gap of ZnO. It means that this is the case of incoming resonance, where the laser line is in resonance with an interband electronic transition. In the present study, we use the 351.1 and 363.8 nm lines of an Ar ion laser for the purpose of exciting samples. The quantum energy of these lines is close to the exciton energy in ZnO, therefore allowing one to investigate the exciton mediated multiphonon resonant Raman scattering under conditions changing from incoming to outgoing resonance. We studied unintentionally doped bulk ZnO crystals and layers, including nanostructured and highly conductive films. The quenching of luminescence and enhancement of Raman scattering in nanostructured layers enabled one to observe and explore the Raman signal in resonant configuration. Furthermore, impurity-induced outgoing RRS was studied in highly conductive ZnO films.

II. EXPERIMENTAL DETAILS

ZnO single crystals were grown from vapor phase without intentional doping. The free electron concentration in bulk crystals was 1×10^{17} cm^{-3} at 300 K. ZnO layers with the thickness ranging from 100 to 500 nm were grown on multilayer and single-layer opal structures using "wet" chemical deposition from a solution of $Zn(NO_3)_2\times nH_2O$ followed by thermal decomposition of the zinc nitrate into zinc oxide. According to the solubility diagram of zinc nitrate in water, it exists only in the form of $Zn(NO_3)_2\times nH_2O$ crystal hydrate, where the amount of water molecules vary from 9 to 1 in the temperature interval from −32 °C to +70 °C. The deposition was performed in the temperature interval from 55 to 70 °C, therefore zinc nitrate contains no more than two water molecules. Silica opal spheres were synthesized through the hydrolysis of tetraethyl

orthosilicate (TEOS) in water-ethanol solution in the presence of ammonium hydroxide following Stöber's method[9] with some modification of the component ratio.[10] Multilayer and single-layer opal structures were fabricated by deposition on nearly vertical substrates during evaporation of the solvent.

In addition, highly conductive ZnO films were prepared by means of a technique derived from chemical vapor deposition and comprising two processes: thermal decomposition of a metalorganic compound and oxidation.[11] The deposition process is carried out in a horizontal reactor. A mixture of argon and oxygen gases at fluxes around 200 cm^3/min passes through the Zn acetylacetonate source that is maintained at fixed temperatures from the interval 80 to 120 °C. During the deposition process the substrate is maintained at definite temperatures from 300 to 400 °C. ZnO films with electron concentration in the range of $(0.2-5)\times 10^{20}$ cm^{-3} were grown by changing the composition of the gas mixture and the temperatures of the source and the substrate. In order to reduce the influence of strains in ZnO layers we used porous InP substrates prepared by electrochemical dissolution[12], following the concept of nanoheteroepitaxy.[13–15]

The samples were excited by the 351.1 and 363.8 nm lines of an Ar^+ SpectraPhysics laser and the emission was analyzed in a quasi-backscattering geometry through a double spectrometer with 1200 grooves/mm gratings assuring a linear dispersion of 0.8 nm/mm. The signal from a FEU-106 photomultiplier with SbKNaCs photocathode working in a photon counting mode was introduced in an IBM computer. The spectral resolution was better than 0.5 meV. The samples were mounted on the cold station of a LTS-22-C-330 workhorse-type optical cryogenic system. The excitation laser beam at 30 mW power was focused to a spot of about 2 mm in diameter resulting in the excitation power density of about 1 W/cm^2.

III. RESULTS AND DISCUSSION

Figure 1 compares the emission spectra of ZnO single crystals excited by the 351.1 and 363.8 nm laser lines. Under both excitations the spectra are dominated by the luminescence of excitons bound to neutral donors. The energy position of the PL lines at 3.363, 3.359, 3.356, and 3.352 eV corresponds to previously reported I_4, I_8, I_9, and I_{10} lines related to donor bound excitons (see, e.g., Refs. 16 and 17). The free A exciton PL band splits into two peaks related to the $\Gamma 5$ and $\Gamma 6$ excitons at 3.3765 and 3.3785 eV. This band is one order of magnitude weaker than the most intensive D^0X line. The other PL bands observed in the spectrum excited by the 351.1 nm laser line are related to the phonon replicas of the X_A and D^0X excitons. Note that the derived phonon energy equals 71 meV which corresponds to the energy of the A_1(LO) phonon.[18–20] With increasing temperature, the intensity of the donor bound exciton luminescence decreases and the luminescence becomes free excitonic. The spectrum excited by the 363.8 nm laser line exhibits two additional emission lines at 3.436 and 3.264 eV. The difference between these values and the excitation quantum energy

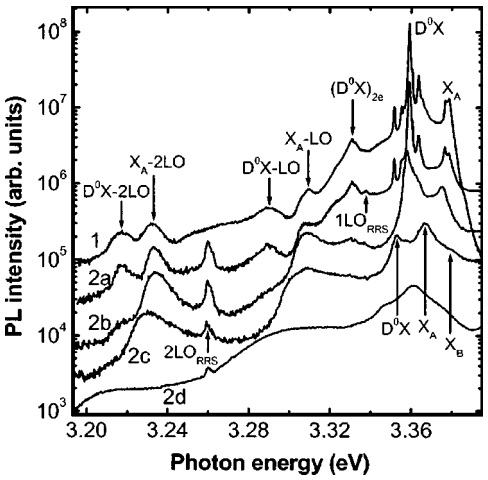

FIG. 1. Emission spectra of ZnO single crystals excited by the 351.1 nm laser line at 10 K (curve 1), and by the 363.8 nm laser line at 10 K (curve 2a), 50 K (curve 2b), 100 K (curve 2c), and 150 K (curve 2d).

(3.407 eV) is one and two times the energy of the A_1(LO) phonon. It means that the emission lines involved originate from the first- and second-order Raman scattering.

To explore the mechanisms of RRS in ZnO we have performed a comparative analysis of the emission spectra in bulk crystals and layers with the thickness ranging from 100 to 500 nm grown on multilayer and single-layer opal structures. Figure 2 shows the emission spectra of 500 nm thick ZnO layer grown on multilayer opal measured at different temperatures under the 363.8 nm laser line excitation. The luminescence spectrum of the layer is similar to that of single crystals, except for one order of magnitude lower intensity and insignificant change in the emission related to donor bound excitons. The low luminescence intensity in ZnO layers provides better conditions for the investigation of the resonant Raman scattering. The modes originating from the photon scattering by first-, second-, and third-order LO

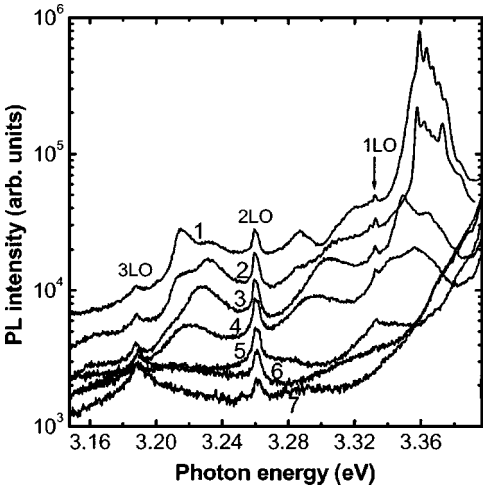

FIG. 2. Emission spectra of thick (500 nm) ZnO layer grown onto bulk opal excited by the 363.8 nm laser line at temperatures 10 K (curve 1), 50 K (curve 2), 100 K (curve 3), 150 K (curve 4), 200 K (curve 5), 250 K (curve 6), and 300 K (curve 7).

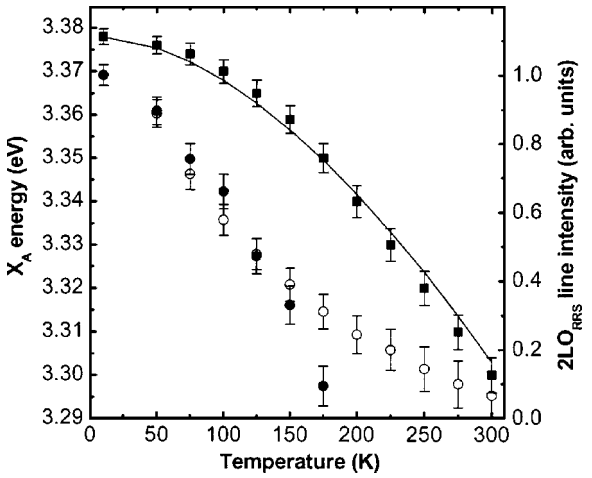

FIG. 3. Temperature dependence of the X_A peak energy (closed squares, left-hand axis) and $2LO_{RRS}$ line intensity (right-hand axis) measured in ZnO single crystals (closed circles) and layers grown on bulk opal (open circles). The solid curve represents the fit to the experimental data by the Varshni formula.

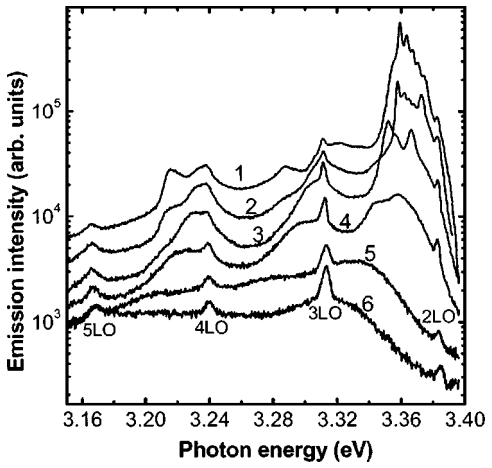

FIG. 4. Emission spectra of thick ZnO layer grown on bulk opal and excited by the 351.1 nm laser line at temperatures 10 K (curve 1), 50 K (curve 2), 100 K (curve 3), 150 K (curve 4), 200 K (curve 5), and 250 K (curve 6).

phonons are clearly observed in the spectrum under resonant excitation by the 363.8 nm laser line (see Fig. 2).

In the previous reports on multiphonon scattering processes in ZnO (Refs. 6–8) the samples were excited by the 325 nm line of a He-Cd laser. The energy of this line is about 440 meV higher than the band gap of ZnO. It means that there is a case of incoming resonance, where the laser line is in resonance with an interband electronic transition. This electronic transition probably occurs between the $A_{5,6}$ valence band and Γ_1 conductance band, as calculated theoretically[21,22] and measured experimentally[23] in wurtzite-type ZnO. In our case, the quantum energy of the 351.1 nm laser line is 100 meV higher than the band gap of ZnO and 160 meV higher than the energy of the free *A* exciton, while the quantum energy of the 363.8 nm laser line is 30 meV lower than the band gap and 30 meV higher than the X_A energy. Since the quantum energy of the 351.1 nm laser line is mismatched with the energy of the X_A exciton, the conditions for the incoming resonant Raman scattering are poorly satisfied. Consequently, the emission spectrum is totally dominated by the luminescence (see curve 1 in Fig. 1). On the other hand, the quantum energy of the 363.8 nm laser line is just in between the band gap and the X_A energy. In such a case, the intensity of the resonant Raman scattering becomes comparable with the luminescence intensity, since the resonance conditions for the incoming RRS are well satisfied. However, with increasing temperature the exciton energy decreases and detuning between the excitation quantum energy and the X_A energy becomes more pronounced. As a result, the intensity of the RRS lines sharply decreases (see Fig. 3), indicating that we deal with the incoming exciton mediated RRS. Note that the experimental data were well fitted (see solid curve in Fig. 3) with the phenomenological Varshni formula[24]

$$E(T) = E_0 - \alpha T^2/(T+\beta)$$

with the parameters $E_0 = 3.378$ eV, $\alpha = 1 \times 10^{-3}$ eV K^{-1}, and $\beta = 900$ K.

Another advantage of low luminescence intensity inherent to layers grown on opals is the possibility to discriminate between the incoming and outgoing regimes of the RRS. As one can see from Fig. 3, the intensity of the $2LO_{RRS}$ line in ZnO layers sharply decreases with the temperature increase up to 150 K, while at higher temperatures the rate of the decrease becomes much slower. We consider this behavior to be related to the transition from the incoming to the outgoing regime of the RRS, since at high temperatures the exciton energy approaches the energy of the photon scattered by second order LO phonons. Moreover, the relatively low PL intensity of layers allows one to investigate the RRS under the 351.1 nm laser line excitation (see Fig. 4). At low temperatures the modes originating from the photon scattering by second- and third-order LO phonons are clearly observed in the spectrum under excitation by the 351.1 nm laser line. With temperature increase, four multiphonon lines are observed in the emission spectrum. As mentioned above, the quantum energy of the 351.1 nm laser line poorly satisfies the conditions for the incoming RRS. On the other hand, the energy of some photons scattered by certain-order LO phonons matches the exciton energy, and we deal with pure outgoing RRS. At 10 K the photon scattered by the second-order LO phonons matches better the exciton energy and the 2LO peak becomes stronger. With increasing temperature, the exciton energy decreases and the photon scattered by the third-order phonons becomes in resonance with the excitons, as illustrated in Fig. 5.

The emission spectrum of thin ZnO films deposited on single-layer opals is absolutely dominated by resonant Raman scattering (see Fig. 6). The following two reasons can be considered to explain the difference between the emission spectra of thick and thin ZnO layers: (i) the nanostructure enhanced resonant Raman scattering in thin layers and (ii) the decrease of the luminescence efficiency due to the surface recombination. As shown recently,[25] ZnO layers with the thickness less than 100 nm deposited on single-layer opals represent actually nanostructures consisting of crystallites with the sizes less than 50 nm deposited through the

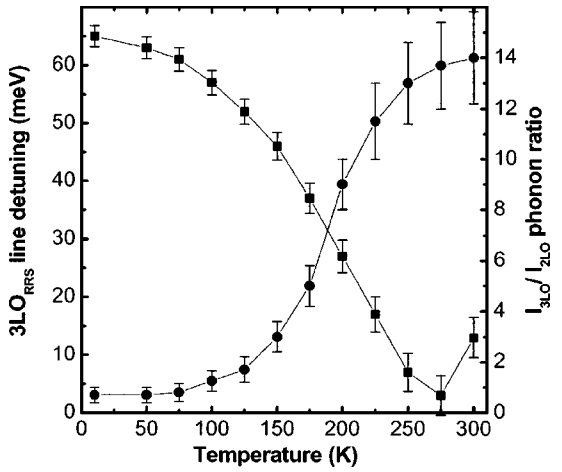

FIG. 5. Temperature dependence of the $3LO_{RRS}$ line detuning (squares, left-hand axis), and of I_{3LO}/I_{2LO} phonon intensity ratio (circles, right-hand axis) measured under 351.1 nm laser line excitation of a thick ZnO layer grown on bulk opal. Lines are to guide the eye only.

openings between the silica spheres, and of crystallites with bigger sizes grown onto the upper surface of the opal spheres, i.e., the single-layer opal works as a nanomask in this case. Apart from strong LO multiphonon lines, weaker lines marked as SO are observed in the emission spectrum of nanostructured layers. The energy of the SO phonons participating in multiphonon scattering proves to be equal to 65 meV. The observed SO phonons may be attributed to Fröhlich-type vibrational modes. When the electromagnetic radiation propagates through nanostructures of polar materials, the polarization of the nanostructure entities in the electric field of the radiation results in the excitation of electrical dipoles vibrating at specific frequencies. These vibrations, not present in bulk material, give rise to new optical modes in Raman scattering located in the frequency gap between the bulk TO and LO optical phonons. The new optical modes, predicted by Fröhlich,[26] have been calculated for

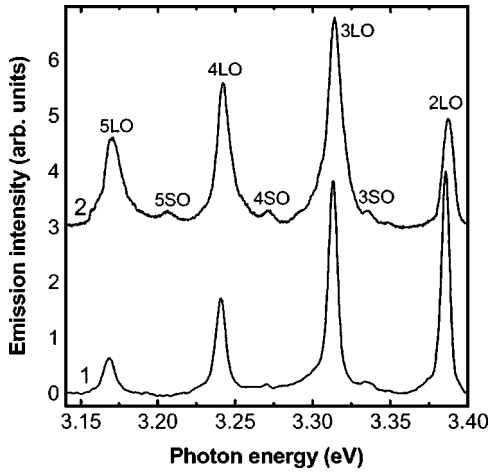

FIG. 6. Emission spectra of thin (100 nm) ZnO film deposited on single-layer opal measured at 10 K (curve 1) and 300 K (curve 2).

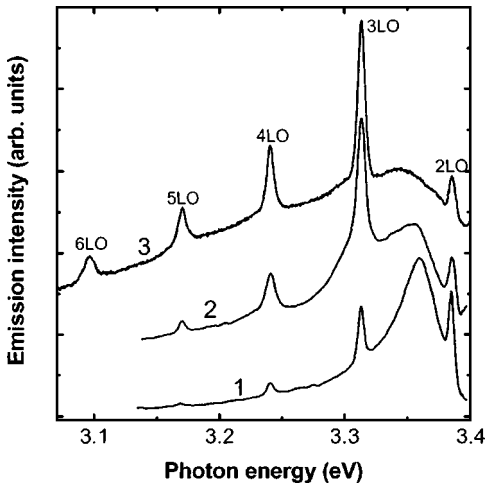

FIG. 7. Emission spectra of ZnO layers with electron concentration 2×10^{19} cm^{-3} (curve 1), 9×10^{19} cm^{-3} (curve 2), and 4.4×10^{20} cm^{-3} (curve 3) measured at 10 K under 351.1 nm laser line excitation.

small ionic crystals of different morphologies by Fuchs and Kliewer[27,28] and have been observed in the infrared absorption and reflectivity spectra of powders by many authors. Fröhlich-type vibrational modes were extensively investigated in nanostructured III-V compounds with zinc blende structure,[29] and recently were observed in wutrzite-type GaN columnar nanostructures.[30] According to calculations performed by Ruppin for small spherical crystals,[31] the efficiency of Raman scattering caused by Fröhlich modes is comparable with that caused by bulk LO and TO phonons only for crystallites with sizes smaller than 100 nm. We assume that the occurrence of SO bands in the resonant Raman scattering is related to Fröhlich modes associated with ZnO crystallites with sizes smaller than 50 nm. In our opinion, the participation of Fröhlich modes in the excitonic multiphonon resonant Raman scattering is indicative of strong exciton-Fröhlich phonon coupling in wurtzite-type ZnO nanocrystals. Note that the interaction between surface-related phonons and confined electron-hole pairs was previously evidenced in resonance Raman scattering of GaP nanocrystals embedded into a glassy matrix.[32]

In order to gain further insight into the nature of resonant Raman scattering in ZnO we have investigated the emission from highly conductive ZnO layers under near band edge resonant excitation. Figure 7 illustrates the emission spectra of three ZnO layers with different electron concentrations under excitation by the 351.1 nm laser line at 10 K. The spectra consist of multiphonon resonant Raman scattering lines superimposed on a broad asymmetric PL band with the maximum at 3.36 eV at low temperatures.

Since a clear correlation exists between the broad PL band and the RRS we will discuss first the possible nature of the 3.36 eV PL band. A characteristic feature of this near-band-gap PL band is the broadening toward the Stokes part of the emission. The width of the PL band varies from 40 to 190 meV, when the carrier concentration increases from 2×10^{19} to 4.4×10^{20} cm^{-3}. There are several mechanisms that may contribute to the broadening of the PL line. The width

of PL lines due to the thermal broadening is expected to be about $3k_BT/2$, i.e., around 1 meV at $T=10$ K, and approximately 40 meV at $T=300$ K. An additional cause of broadening could be homogeneous and inhomogeneous strain related to lattice parameter and thermal expansion coefficient mismatches between substrate and film. According to the concept of nanoheteroepitaxy,[13–15] it is expected that the nucleation of the film on nanoporous substrates will significantly reduce the strain energy. Indeed, the analysis of excitonic PL lines in ZnO layers with low carrier concentration grown on nanoporous substrates showed that the films are free of strain. Thus, neither thermal broadening nor substrate-film mismatches determine PL line broadening at low temperatures.

One commonly claimed mechanism for the broadening of the PL lines at high carrier concentrations is the Burstein-Moss effect, which was found to have significant impact on recombination phenomena in some heavily doped III-V compounds.[33,34] The origin of this effect is the shift of the Fermi level above the bottom of the conduction band as the doping level increases beyond the degeneracy limit. The PL line was found to shift to higher energies, scaling as a 2/3 power of the net carrier concentration. Thus, the shift of the PL line follows that of the Fermi level. Furthermore, due to the indirect transitions (violating the **k** selection rule) between the filled states in the conduction band and acceptor-like states at the top of the valence band, the width of the PL line was found empirically to be nearly 3/4 of the value of (E_F-E_C).

The analysis of the data presented in Fig. 7 suggests that the Burstein-Moss effect is not the appropriate one to explain the PL behavior in our case. First, no upward frequency shift of the PL line with increase of the doping level is observed. Second, the dependence of the full width at half maximum (FWHM) on the carrier concentration (n_e) is much weaker than $(n_e)^{2/3}$ as expected for the Burstein-Moss effect (see Fig. 8). The FWHM in our most highly conductive samples ($n_e=4.4\times10^{20}$ cm^{-3}) equals 190 meV. This value proves to be significantly smaller than the value of FWHM predicted by the Burstein-Moss model, which is of about $3(E_F-E_C)/4 \sim 410$ meV. Note that the $(E_F\text{-}E_C)$ value for $n_e=4.4\times10^{20}$ cm^{-3} determined taking into account the nonparabolicity of the ZnO conduction band equals 550 meV.[35]

We believe that the PL band with the maximum at 3.36 meV ($T=10$ K) is mainly due to direct transitions of electrons between the conduction to valence band tails. The broadening of the PL band involved can be accounted for by the broadening of the band edges due to potential fluctuations induced by the high concentration of intrinsic defects. The width of the band tails, and the dependence of the FWHM of the PL band on carrier concentration can be calculated using the model for broadening of impurity bands in heavily doped semiconductors developed by Morgan.[36] The model was successfully used recently to account for the broadening of near-band-gap luminescence lines in GaN films doped by silicon.[37] We applied this model to ZnO layers since the parameters of GaN and ZnO are nearly the same. In particular, for both compounds the reported values for the dielectric constant and electron effective mass are in the range of 8 to 9 (Refs. 20,38) and $(2.1-2.5)m_0$,[39–41] respectively. Figure 8 presents the measured FWHM of the PL band for samples with different electron concentrations along with the calculated curve. One can note a rather good agreement between experimental and calculated data.

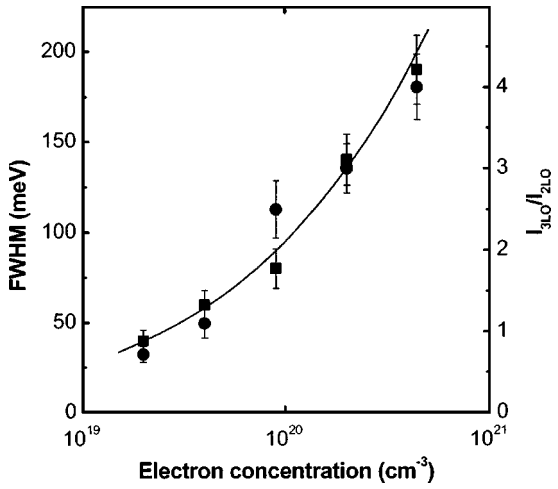

FIG. 8. FWHM of the 3.36 eV PL band measured at $T=10$ K (squares, left-hand axis), and the intensity ratio of 3LO to 2LO phonon lines in the RRS (circles, right-hand axis) as a function of carrier concentration. The solid line represents the result of FWHM calculations according to the Morgan model.

Let us discuss the microscopic origin of the impurity responsible for the potential fluctuations. Taking into account the deviation from stoichiometry towards oxygen deficiency assured by the technological conditions and confirmed by the energy dispersive x-ray analysis of the layers, one can suggest that the potential fluctuations are caused by intrinsic defects related to oxygen deficiency. Oxygen vacancies and zinc interstitials are the most probable donor-type intrinsic defects, since their formation enthalpy is low and they are abundant in Zn-rich conditions, as reported recently.[42,43] Oxygen vacancy is a deep donor, while zinc interstitial is a shallow donor.[42] Thus, one can assume that the broadening of near-band-gap luminescence in our layers is due to high concentration of Zn_i defects.

Figure 8 also presents the intensity ratio of 3LO to 2LO phonon lines in the resonant Raman scattering spectrum (I_{3LO}/I_{2LO}) as a function of carrier concentration. One can notice a clear correlation between the dependence of FWHM and I_{3LO}/I_{2LO} upon electron concentration. The correlation between the FWHM of the luminescence band and the I_{3LO}/I_{2LO} ratio in resonant Raman scattering is indicative of relation between the broadening of the band edges due to potential fluctuations and the mechanisms of resonant Raman scattering. This assumption is supported by the analysis of the temperature dependence of the emission from highly conductive ZnO films. Figure 9 shows the emission spectra of a ZnO layer with electron concentration 9×10^{19} cm^{-3} measured at temperatures from 10 to 300 K under the excitation by 351.1 and 363.8 nm laser lines. The spectra excited by 351.1 nm laser line consist of resonant Raman scattering lines superimposed on the PL band, while the emission excited by 363.8 nm laser line is dominated by RRS at all

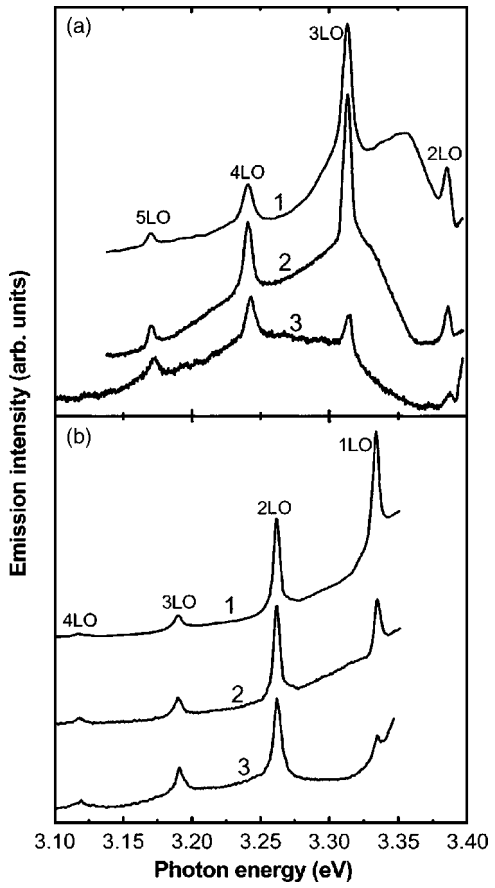

FIG. 9. Emission spectra of ZnO layer with electron concentration 9×10^{19} cm^{-3} excited by 351.1 nm (a) and 363.8 nm (b) laser lines at 10 K (curve 1), 250 K (curve 2), and 300 K (curve 3).

temperatures. Figure 10 illustrates the temperature dependence of the intensity ratio of phonon lines along with the temperature dependence of the position and the FWHM of the luminescence band. One can see that with increasing temperature the PL band exhibits a downward energy shift and broadens. At the same time, the temperature increase leads to the redistribution in the intensity of RRS lines in favor of those which energy better matches the position of the luminescence band at the respective temperature. At low temperatures, the position of the PL band is more appropriate to the energy of photons scattered by third-order LO phonons when exited by the 351.1 nm laser line, and to the energy of photons scattered by first-order LO phonons when excited by the 363.8 nm laser line. Indeed, as one can see from Fig. 9, the respective RRS lines are more intensive at low temperatures. With the temperature increase, the PL band shifts towards the position of the 4LO RRS line under the 351.1 nm laser line excitation, and towards the position of the 2LO RRS line under the 363.8 nm laser line excitation. The spectra presented in Fig. 9 clearly demonstrate that the redistribution takes place in favor of those RRS lines with increasing temperature. The position of the 3LO RRS line under the 351.1 nm laser line excitation coincides with the maximum of the PL band at 250 K, leading to a considerable intensification of this line, see curve 2 in Fig. 9(a). At room temperature the position of the 2LO RRS line under the 363.8 nm

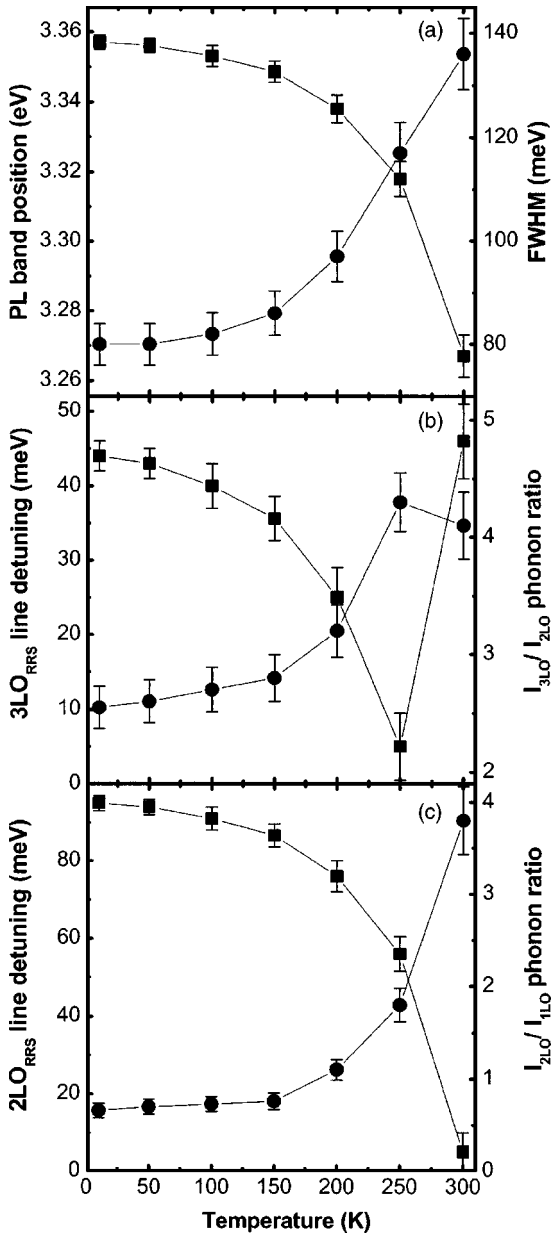

FIG. 10. Temperature dependence of PL (a) and multiphonon RRS excited by 351.1 nm laser line (b) and 363.8 nm laser line (c) in ZnO layer with electron concentration $n=9\times10^{19}$ cm^{-3}. In section (a) squares stand for the PL band position (left-hand axis), and circles correspond to FWHM (right-hand axis). In section (b) squares stand for the $3LO_{RRS}$ line detuning (left-hand axis), and circles correspond to I_{3LO}/I_{2LO} phonon intensity ratio (right-hand axis). In section (c) squares stand for the $2LO_{RRS}$ line detuning (left-hand axis), and circles correspond to I_{2LO}/I_{1LO} phonon intensity ratio (right-hand axis). Lines are to guide the eye only.

laser line excitation coincides with the maximum of the PL band at 300 K, which results in a predominant income from the second-order LO phonon scattering, as illustrated by curve 3 in Fig. 9(b). The analysis presented in Fig. 10 demonstrates the interdependence between the detuning of multiphonon RRS lines from the energy position of the PL line and the intensity of these lines in the RRS spectrum. Therefore, the resonant Raman scattering in highly conductive

ZnO films occurs also in outgoing regime, but the mechanism seems to be more complicated.

Our experimental results on resonant Raman scattering in ZnO single crystals and unintentionally doped layers are in agreement with the "cascade model" proposed by Martin and Varma.[44] The resonance features in exciton-mediated multiphonon Raman scattering can be explained in the framework of a hot exciton cascade relaxation process comprising the following steps: (i) the absorption of the incident photon ($\hbar\omega_i$) with the excitation of an exciton, (ii) the relaxation of this exciton into lower energy states with successive emission of LO phonons through a cascade-type process, and (iii) the radiative recombination of the exciton with the emission of the scattered photon ($\hbar\omega_s \cong \hbar\omega_i - n\hbar\omega_{\mathrm{LO}}$).

On the other hand, in highly conductive ZnO layers with a high concentration of impurities (native defects), the impurities (native defects) can also contribute to the outgoing multiphonon RRS. Several mechanisms have been previously proposed to account for the impurity enhanced Raman scattering: (i) the contribution from the intraband matrix element of the Fröhlich electron-phonon interaction,[45–48] (ii) excitons bound to impurities as intermediate electronic states,[47–49] (iii) impurity-induced mechanism in which the exciton scatters twice: once due to the electron-phonon interaction and again due to the electron impurity interaction.[50] The contribution from the third mechanism is significant for one-LO-phonon scattering, but it can be neglected for scattering by two and more phonons.[48] On the other hand, serious breakdown of the wave-vector conservation may occur in highly conductive layers due to scattering by random impurities. The relaxation of the quasi-momentum conservation allows phonons with larger wave-vectors to participate in the Raman scattering. These larger wave vectors greatly enhance the intraband Fröhlich contribution, and therefore increase the corresponding scattering cross section. The enhancement of outgoing RRS intensity with impurity inducement has been recently observed in impurity-implanted wurtzite GaN.[51]

IV. CONCLUSIONS

Good correlation between 363.8 nm laser line quantum energy and ZnO exciton energy at low temperatures results in a strong incoming multiphonon RRS in zinc oxide single crystals and unintentionally doped layers. The increasing detuning between the 363.8 nm laser line energy and the exciton energy, and the decreasing detuning between the exciton energy and the energy of photon scattered by second-order LO phonons with the temperature increase leads to the transition from incoming to outgoing RRS. Under the 351.1 nm laser line excitation, the RRS exhibits evident features of outgoing resonance due to the significant mismatch between the laser line quantum energy and the exciton energy. The variation of resonant conditions caused by temperature induced shift of the exciton energy leads to the redistribution in the intensity of lines in outgoing RRS in favor of the lines which energy better matches the exciton energy at the respective temperature. The quenching of the luminescence and the enhancement of Raman scattering in nanostructured ZnO layers grown on single-layer opals enable one to explore the Raman signal in resonant configuration thus making possible to observe multiphonon RRS by Fröhlich-type vibrational modes along with RRS by LO phonons. The emission spectrum of highly conductive ZnO films grown under deviation from stoichiometry toward oxygen deficiency consists of a broad PL band superimposed on RRS lines. The occurrence of PL is attributed to tailing of the density of states caused by potential fluctuations due to randomly distributed impurities (or intrinsic defects). On the other hand, scattering by randomly distributed impurities leads to serious breakdown of the wave-vector conservation. This phenomenon, in its turn, results in enhanced intraband Fröhlich contribution to Raman scattering efficiency and occurrence of outgoing RRS with impurity inducement.

ACKNOWLEDGMENTS

This work was supported by INTAS under Grant No. 01-0796 and by CRDF under Grant No. MR2-995. ISSP authors are grateful for the financial support received from the Russian Foundation for Basic Research (Project No. 01-02-97024) and from the Russian Federation Government under Contract No. 40.012.1.1.11.54.

*Email address: tiginyanu@mail.md

[1] T. Miyata, T. Minami, K. Saikai, and S. Takata, J. Lumin. **60**, 926 (1994).
[2] S. Nakamura, T. Mukai, and M. Senoh, Appl. Phys. Lett. **64**, 1687 (1994).
[3] D. M. Bagnall, Y. F. Chen, Z. Zhu, T. Yao, S. Koyama, M. Y. Shen, and T. Goto, Appl. Phys. Lett. **70**, 2230 (1997).
[4] M. Zamfirescu, A. Kavokin, B. Gill, G. Malpuech, and M. Kaliteevski, Phys. Rev. B **65**, 161205(R) (2002).
[5] P. Y. Yu and M. Cardona, *Fundamentals of Semiconductors* (Springer-Verlag, Berlin, 1996).
[6] J. F. Scott, Phys. Rev. B **2**, 1209 (1970).
[7] X. T. Zhang, Y. C. Liu, Z. Z. Zhi, J. Y. Zhang, Y. M. Lu, D. Z. Shen, W. Xu, G. Z. Zhong, X. W. Fan, and X. G. Kong, J. Phys. D **34**, 3430 (2001).
[8] H. T. Ng, B. Chen, J. Li, J. Han, M. Meyyappan, J. Wu, S. X. Li, and E. E. Haller, Appl. Phys. Lett. **82**, 2023 (2003).
[9] W. Stöber, A. Fink, and E. Bohn, J. Colloid Interface Sci. **26**, 62 (1968).
[10] V. M. Masalov, K. A. Aldushin, P. V. Dolganov, and G. A. Emel'chenko, Phys. Low-Dimens. Semicond. Struct. **5-6**, 45 (2001).
[11] M. Purica, E. Budianu, and E. Rusu, Microelectron. Eng. **51-52**, 425 (2000).
[12] S. Langa, I. M. Tiginyanu, J. Carstensen, M. Christophersen, and H. Föll, Appl. Phys. Lett. **82**, 278 (2003).

[13] D. Zubia and S. D. Hersee, J. Appl. Phys. **85**, 6492 (1999).
[14] D. Zubia, S. H. Zaidi, S. R. J. Brueck, and S. D. Hersee, Appl. Phys. Lett. **79**, 858 (2000).
[15] J. Liang, S.-K. Hong, N. Kouklin, R. Beresford, and J. M. Xu, Appl. Phys. Lett. **83**, 1752 (2003).
[16] D. C. Reynolds, C. W. Litton, and T. C. Collins, Phys. Rev. **140**, A1726 (1965).
[17] B. K. Meyer, H. Alves, D. M. Hofmann, W. Kriegseis, D. Forster, F. Bertram, J. Christen, A. Hoffmann, M. Strassburg, M. Dwworzak, U. Haboeck, and A. V. Rodina, Phys. Status Solidi B **241**, 231 (2004).
[18] J. M. Calleja and M. Cardona, Phys. Rev. B **16**, 3753 (1977).
[19] F. Decremps, J. Pellicer-Porre, A. Marco Saitta, J.-C. Chervin, and A. Polian, Phys. Rev. B **65**, 092101 (2002).
[20] N. Ashkenov, B. N. Mbenkum, C. Bundesmann, V. Riede, M. Lorenz, D. Speman, E. M. Kaidashev, A. Kasic, M. Schubert, M. Grundmann, G. Wagner, H. Neumann, V. Darakchieva, H. Arwin, and B. Monemat, J. Appl. Phys. **93**, 126 (2003).
[21] P. Schroer, P. Kruger, and J. Pollmann, Phys. Rev. B **47**, 6971 (1993).
[22] W. R. L. Lambrecht, S. Limpijumnong, and B. Segall, MRS Internet J. Nitride Semicond. Res. **4S1**, G6.8 (1999).
[23] R. T. Girard, O. Tjernberg, G. Chiaia, S. Soderholm, U. O. Karsson, C. Wigren, H. Nylen, and I. Lindau, Surf. Sci. **373**, 409 (1997).
[24] Y. P. Varshni, Physica (Amsterdam) **34**, 149 (1967).
[25] A. N. Gruzintsev, V. T. Volkov, G. A. Emelchenko, I. A. Karpov, V. M. Masalov, G. M. Mikhaĭlov, and E. E. Yakimov, Semiconductors **37**, 314 (2003).
[26] H. Fröhlich, *Theory of Dielectrics* (Clarendon Press, Oxford, 1949).
[27] R. Fuchs and K. L. Kliewer, Phys. Rev. **140**, A2076 (1965).
[28] R. Fuchs and K. L. Kliewer, J. Opt. Soc. Am. **58**, 319 (1967).
[29] See, for instance, I. M. Tiginyanu, G. Irmer, J. Monecke, and H. L. Hartnagel, Phys. Rev. B **55**, 6739 (1997); A. Sarua, G. Irmer, J. Monecke, I. M. Tiginyanu, C. Schwab, J.-J. Grob, and H. L. Hartnagel, J. Appl. Phys. **88**, 7006 (2000); V. V. Ursaki, I. M. Tiginyanu, P. C. Ricci, A. Anedda, E. V. Foca, and N. N. Syrbu, J. Phys.: Condens. Matter **13**, 4579 (2001).
[30] I. M. Tiginyanu, A. Sarua, G. Irmer, J. Monecke, S. M. Hubbard, D. Pavlidis, and V. Valiaev, Phys. Rev. B **64**, 233317 (2001).
[31] R. Ruppin, J. Phys. C **8**, 1969 (1975).
[32] Al. L. Efros, A. I. Ekimov, F. Kozlowski, V. Petrova-Koch, H. Schmidbaur, and S. Shumilov, Solid State Commun. **78**, 853 (1991).
[33] J. D. De-Sheng, Y. Makita, K. Ploog, and H. G. Queisser, J. Appl. Phys. **53**, 999 (1982).
[34] V. A. Vilkotskii, D. S. Domanevskii, R. D. Kakanakov, V. V. Krasovskii, and V. D. Tkachev, Phys. Status Solidi A **91**, 71 (1978).
[35] D. L. Young, T. J. Coutts, V. I. Kaydanov, A. S. Gilmore, and W. P. Mulligan, J. Vac. Sci. Technol. A **18**, 2978 (2000).
[36] T. N. Morgan, Phys. Rev. **139**, A343 (1965).
[37] E. Iliopoulos, D. Doppalopudi, H. M. Ng, and T. D. Moustakas, Appl. Phys. Lett. **73**, 375 (1998).
[38] T. Deguchi, D. Ichiryu, K. Toshikawa, K. Sekiguchi, T. Sota, R. Matsuo, T. Azuhata, M. Yamaguchi, T. Yagi, S. Chichibu, and S. Nakamura, J. Appl. Phys. **86**, 1860 (1999).
[39] S. Syed, J. B. Heroux, Y. J. Wang, M. J. Manfra, R. J. Molnar, and H. L. Stormer, Appl. Phys. Lett. **83**, 4553 (2003).
[40] Y. Imanaka, M. Oshikiri, K. Takahana, T. Takamasu, and G. Kido, Physica B **298**, 211 (2001).
[41] M. Oshikiri, F. Aryasetiawan, Y. Imanaka, and G. Kido, Phys. Rev. B **66**, 125204 (2002).
[42] S. B. Zhang, S.-H. Wei, and A. Zunger, Phys. Rev. B **63**, 075205 (2001).
[43] E. Oba, S. R. Nishitani, S. Isotani, H. Adachi, and I. Tanaka, J. Appl. Phys. **90**, 824 (2001).
[44] R. M. Martin and C. M. Varma, Phys. Rev. Lett. **26**, 1241 (1971).
[45] D. C. Hamilton, Phys. Rev. **188**, 1221 (1969).
[46] R. M. Martin and T. C. Damen, Phys. Rev. Lett. **26**, 86 (1971).
[47] J. Menendez and M. Cardona, Phys. Rev. B **31**, 3696 (1985).
[48] J. Menendez, M. Cardona, and L. K. Vodopyanov, Phys. Rev. B **31**, 3705 (1985).
[49] P. J. Colwell and M. V. Klein, Solid State Commun. **8**, 2095 (1976).
[50] A. A. Gogolin and E. I. Rashba, Solid State Commun. **19**, 1177 (1970).
[51] W. H. Sun, S. J. Chua, L. S. Wang, and X. H. Zhang, J. Appl. Phys. **91**, 4917 (2002).